
Title:
Implicit-tuning signal quantified through a tri-experiment design in a legacy spectral GCM

Author: Dmitrii Vokhmintsev
ORCID: `https://orcid.org/0000-0003-4531-118X`
Affiliation: Independent Researcher, Saint Petersburg, Russia
Corresponding e-mail: dmitry.vohmincev@gmail.com

Target peer-review journal: *Journal of Advances in Modeling Earth Systems* (JAMES), American Geophysical Union (AGU)
Manuscript status: Submitted for peer review on 2026-06-14 (manuscript ID `2026MS006158`)

Preprint version: v1, 2026-06-14

Replication package (data, code, analysis):
`https://doi.org/10.5281/zenodo.20447240`

Companion preprint (parallelization study, submitted to JPDC):
`https://doi.org/10.2139/ssrn.6608580`

Implicit-tuning signal quantified through a tri-experiment design in a legacy spectral GCM

Dmitrii Vokhmintsev[1]*

[1]Independent Researcher, Saint Petersburg, Russia

Key points

- An unintended inter-latitude memory leak in the vertical-exchange parameterization shifts the 30-year MGO GCM climatology
- Strict bitwise reproducibility across thread counts is shown to be a deductive consequence of three implementation conditions
- Both candidate fixes improve simulated surface temperature but enlarge cloud and radiation biases against observations

*dmitry.vohmincev@gmail.com

Abstract

We quantify the climate response of the MGO atmospheric general circulation model (MGO-03 T42L25) to two alternative implementations of a structural fix in the vertical-exchange parameterization. A companion parallelization study (under review) identifies an unintended inter-latitude state leakage through `SAVE`-persistent working arrays in the boundary-layer scheme. Here we contrast the legacy code (REF) against two candidate repairs—zero-reinitialization at each latitude (CTRL_A) and per-latitude snapshot/restore of the prior state (CTRL_B)—in a three-member initial-condition ensemble of 30-year AMIP-style integrations (1979–2008), and evaluate the simulated climatologies against ERA5, CERES EBAF, GPCP, and ISCCP-H observational datasets. Pairwise comparisons with pooled-paired t-tests across the ensemble, an effective-sample-size correction for temporal autocorrelation, and Benjamini–Hochberg control of the false discovery rate at $q = 0.05$ reveal that (i) the choice between the two implementations—contrasted at identical compilation settings (CTRL_B−CTRL_A)—is itself FDR-significant in 20.34 % of T42 cells in annual surface air temperature, exceeding the CTRL_B−REF leak-elimination signal in both area-weighted amplitude and FDR-significant spatial extent; (ii) both repairs enlarge the model bias in radiation and cloud cover against observations relative to REF, a pattern consistent with the hypothesis that the legacy configuration was implicitly tuned against the leaky baseline; the ensemble establishes the signal's robustness but does not isolate the mechanism among several plausible alternatives. We additionally document that the legacy implementation is not thread-reproducible across OpenMP partitions. A formal bit-reproducibility theorem, identifying three implementation conditions under which OpenMP parallelization of the model is bitwise reproducible by construction, is presented in the Supporting Information.

Plain Language Summary

Climate models of Earth's atmosphere run on parallel computers with many CPU cores working simultaneously. We describe a hidden bug in one component of the MGO climate model—the calculation of how air mixes vertically near the surface—in which the calculation was unintentionally remembering values from one latitude band to the next. We test two different ways of fixing this bug in 30-year simulations and compare the results with satellite and reanalysis observations. The two fixes produce slightly different climates, and the choice between them matters at climate scale for several quantities.

Both fixes improve the simulated surface temperature against observations but degrade simulated cloud cover and radiation, suggesting that the legacy model was indirectly tuned to compensate for the bug. We also document that the uncorrected version gives different answers when run on different numbers of CPU cores, while the corrected versions do not—a property that we prove must follow from three specific implementation conditions, established in a companion technical note.

1 Introduction

Modern atmospheric general circulation models (GCMs) are routinely executed on shared-memory parallel hardware, where increasing the number of OpenMP threads is expected to yield speedup without altering the simulated climate. This expectation rests on an implicit assumption: that the parallel implementation is bitwise reproducible across thread counts, and that each parallel kernel has well-defined per-iteration semantics. The assumption can fail silently in legacy codes that rely on Fortran `SAVE` attributes for working arrays, because what is an innocuous side-effect in a serial implementation—that an array retains its value across calls—becomes an undefined inter-iteration coupling under thread-static storage.

The bitwise reproducibility of climate simulations under parallelization has a substantial history. Rosinski and Williamson (1997) characterized the growth of rounding-sized initial errors in CCM2 and introduced a port-validation strategy for atmospheric GCMs, identifying physical parametrizations as the source of fast error amplification. Baker et al. (2015) subsequently introduced ensemble-based consistency tests for the Community Earth System Model, motivated by the observation that common events in a model's development life cycle—porting to new hardware, compiler upgrades, and changes in processor count—routinely break bit-for-bit identity and call for statistical equivalence tests when strict reproducibility cannot be assumed. This approach has since been adopted across major modelling centres: Massonnet et al. (2020) established a statistical replicability protocol for EC-Earth3, adopted by a consortium of 27 institutions; Schär et al. (2020) measured that enforcing bit reproducibility in the COSMO regional model slows the CPU implementation by 37 % and the GPU implementation by 13 % relative to their respective non-reproducible baselines; and Dörfler et al. (2022) documented that, in part because of such costs, bit reproducibility is generally not enforced in oper-

ational weather and climate models. Structural conditions under which a parallel GCM can be guaranteed strictly bitwise reproducible *by construction* are rarely articulated.

The companion paper Vokhmintsev (2026a) demonstrates that strict bit-identity across $N \in \{1, 2, 4, 8, 12, 16, 32\}$ threads is achievable for the MGO atmospheric GCM at T42L25 resolution, on two distinct hardware platforms (AMD Zen 5 and Intel Ivy Bridge-EP). Achieving this property required identifying and fixing a number of inter-iteration state leaks in the legacy code. The most consequential was the unintended persistence of vertical-exchange working arrays across latitudes, fixed by the per-latitude reset `VE_JRESET`: twenty-five `SAVE`-attributed working arrays in the vertical-exchange parameterization were, prior to the fix, retaining their values from one latitude J to the next via Fortran `SAVE`-persistence. Under serial execution this constituted a hidden inter-latitude coupling; under thread-parallel execution it became a thread-dependent quasi-randomness, because the partition of latitudes across threads depends on the thread count.

The choice of T42L25 horizontal resolution in the present study is methodologically deliberate. T42L25 is the resolution at which parallelization-induced state-leakage and its climate consequences can be characterized in clean form, prior to the additional confounds (memory-bandwidth-limited execution, NUMA effects, and resolution-dependent numerical artifacts) that emerge at higher horizontal resolutions. Companion work at T63L25 and T106L25 is in preparation; the present results establish necessary conditions for parallel reproducibility and identify the implementation-choice signal that will be re-verified at those resolutions in dedicated follow-up papers.

While the companion paper establishes bit-identity, it leaves open the question of climate response: did the structural fix to vertical exchange substantively change the model's simulated climate, and if so, in what direction? An exploratory one-month integration showed a global-mean T_{2m} shift of -0.31 K and a southern-hemisphere low-cloud shift of -11.4 percentage points, both well above natural one-month variability. A one-month signal, however, cannot distinguish a transient adjustment from a persistent climate change, nor can it quantify the statistical significance of the response against the internal variability of the model.

The present paper quantifies the long-term climate response of two alternative repairs of this inter-latitude leak through a three-member initial-condition ensemble of 30-year AMIP-style integrations (1979–2008) of the legacy REF code and of two structurally distinct corrections, CTRL_A (zero reinitialisation of the working arrays at each latitude) and CTRL_B (per-latitude snapshot/restore of the prior state). Each configuration is run as a three-member ensemble whose members differ only by a round-off-level perturbation of the initial temperature field, so that the spread among members measures the model's internal variability and the ensemble mean isolates the deterministic response to the code change. Simulated climatologies are compared against ERA5 (Hersbach et al., 2020), CERES EBAF (Loeb et al., 2018), GPCP (Adler et al., 2018), and ISCCP-H HGM (Young et al., 2018) observational datasets. We additionally document an empirical property of the legacy code that, to our knowledge, has not been quantified before: the legacy implementation is not only physically suspect (the `SAVE`-persistence is best read, on structural inspection of the routine, as an unintended carry-over of working-array state between latitudes rather than a documented per-latitude memory mechanism) but also numerically not thread-reproducible—different OpenMP thread counts yield different climate trajectories on the same hardware-compiler configuration. This is offered as additional evidence that the fix is structural rather than cosmetic.

The paper is organised as follows. Section 2 describes the model, the experimental design (the triple-experiment contrast REF versus CTRL_A versus CTRL_B), the statistical methodology, and the observational datasets. Section 3 summarises the bitwise reproducibility framework that motivates the experimental design; the formal theorem and its proof are deposited in the Supplementary Information. Section 4 presents the model-versus-model contrasts for the three pairwise comparisons. Section 5 presents the model-versus-observations comparison against the four observational datasets. Section 6 interprets the results in the context of the implicit-tuning literature and acknowledges the limitations of the triple-experiment design. Section 7 synthesises the implications for community climate-model development.

2 Model and Methods

2.1 The MGO atmospheric general circulation model

The simulations reported here use the MGO atmospheric general circulation model, version MGO-03, in its T42L25 spectral configuration (Meleshko et al., 2014; Shneerov et al., 2001). The horizontal spectral truncation is triangular at total wavenumber 42, transformed onto a 64×128 Gaussian grid; the vertical discretization uses 25 sigma levels, with the topmost full level at $\sigma = 0.005$ (approximately 5 hPa for a 1000 hPa surface-pressure reference). The dynamical core is a semi-implicit spectral-transform formulation (Bourke, 1974) with leapfrog time stepping and Robert–Asselin time filter; physics is called on the Gaussian grid each physics time step.

The physical-parameterization suite, inherited from the canonical MGO-2 production code (Shneerov et al., 2001), comprises a level-2.5 Mellor–Yamada planetary boundary layer (Mellor & Yamada, 1982, 1974; Holtslag & Boville, 1993), a mass-flux deep-convection scheme of the Tiedtke family (Tiedtke, 1989; Bechtold et al., 2008) (alternative mass-flux formulations from the Arakawa–Schubert lineage are represented by Zhang and McFarlane (1995)), a prognostic large-scale-condensation cloud scheme (Sundqvist et al., 1989; Tiedtke, 1993) diagnosing two cloud categories (convective and stratiform) together with a separate subinversion stratocumulus branch in the lower tier, a shortwave and longwave radiation scheme based on the Goody statistical band model with Curtis–Godson scaling for atmospheric inhomogeneity, with prescribed greenhouse-gas concentrations and observed aerosol monthly climatologies, an interactive land-surface model with prescribed vegetation and a four-layer soil-moisture diffusion scheme, and a thermodynamic slab-ocean component (deactivated in the present configuration; the boundary conditions used in this study are described in Section 2.2). The MGO-03 configuration is described in its canonical model-documentation paper (Meleshko et al., 2014), building on the original MGO-2 description (Shneerov et al., 2001), and has been applied to equilibrium climate sensitivity studies for CO_2 doubling (Bulgakov et al., 2008).

The structural code modification under study—the per-latitude reinitialization `VE_JRESET` of 25 working arrays in the vertical-exchange routine `ve_r2`—is described in detail in the companion parallelization paper (Vokhmintsev, 2026a). Two can-

didate implementations of the reinitialization are contrasted in the present work: *Variant A* (zero reinitialization) sets all 25 working arrays to zero at the start of each call to `ve_r2`, with the exception of two of the arrays which are initialized to unity rather than zero to maintain consistency with a nonzero-default convention identified in the integration loop of the legacy routine; *Variant C* (per-latitude snapshot/restore) introduces a dedicated memory module (`VE_MEM_MOD`) which preserves the working-array state per latitude index J between successive calls within a time step. Variant C therefore preserves a physically meaningful previous-time-step memory per latitude, where Variant A discards it.

No "Variant B" is defined for the vertical-exchange reinitialization: the labels A and C are inherited from a wider determinism-recovery enumeration of candidate state-handling strategies, of which only these two were retained for `ve_r2`.

2.2 Experimental design

We adopt an AMIP-style protocol (Gates et al., 1999; Eyring et al., 2016) with the slab-ocean component disabled. Boundary conditions are prescribed monthly sea-surface temperature, sea-ice concentration, and sea-ice thickness from the `CMIPMOD` boundary-condition dataset for 1979–2008 (documented in the replication package (Vokhmintsev, 2026b)), together with well-mixed greenhouse-gas concentrations and aerosol monthly climatologies. The experiment is executed under the script `slab-693_r4`; the script name retains historical nomenclature from an earlier slab-ocean variant and does not indicate an active slab in the present runs. The boundary conditions are identical across all three experiments considered below; this AMIP-shared forcing produces a paired design in which a large fraction of the internal-variability variance cancels under pairwise subtraction.

The choice of AMIP-style prescribed-SST forcing rather than interactive ocean coupling is methodologically appropriate for the present scientific question. Inter-experiment attribution of an atmospheric implementation choice requires identical boundary conditions across the configurations contrasted; an interactive ocean would introduce configuration-dependent sea-surface temperature and sea-ice differences that would confound the attribution of any climate response to the vertical-exchange state handling. The CFMIP-3 protocol of Webb et al. (2017) similarly uses

prescribed-SST atmospheric experiments to isolate cloud and radiation feedback components from ocean-coupling effects, and the AMIP framework of Gates et al. (1999) remains the canonical inter-comparison protocol for atmosphere-only process studies in the CMIP6 era (Eyring et al., 2016).

Three model configurations, each integrated as a three-member initial-condition ensemble of 30-year runs covering 1979-01 to 2008-12, are performed:

- **REF**: the legacy code with the inter-J state leakage intact (25 `SAVE+THREADPRIVATE` arrays in the vertical-exchange routine retain values across the latitude loop), built at commit `2ae84cec`.
- **CTRL_A**: the Variant A (zero-reinitialization) fix, built at commit `4a7dc6c4` of the branch `paper2-gmd-ve-jreset-climate`.
- **CTRL_B**: the Variant C (per-J snapshot/restore) fix, built at commit `d5b981ed` of the branch `paper2-variant-c`.

The three-member ensembles were completed on 2026-05-21; the full per-member build provenance (commit hash, compiler version, compilation flags, and output `MD5` checksums) is distributed with the replication package (Vokhmintsev, 2026b).

The three configurations differ in the treatment of the working-array state in `ve_r2` between consecutive latitudes of the physics loop; all other model code and boundary conditions are identical. The REF executable was compiled with `-O2`, whereas the two fix configurations were compiled with `-O2 -march=native`. We verified by direct measurement that this compilation-flag difference does not alias the reported signal: re-running REF with `-O2 -march=native` and differencing against the `-O2` REF ensemble member-by-member yields a global-mean `tas` flag effect of +0.007 K—an order of magnitude below the CTRL_A−REF signal of +0.067 K ($\approx$ 11 % of the signal) and within the inter-member ensemble spread of 0.010 K.[1] The reported climatological differences are therefore attributable to

[1] A two one-sided tests (TOST) equivalence assessment on the three initial-condition-paired flag differences (−0.012, +0.014, +0.019 K; mean +0.007 K) does not formally establish equivalence at $N = 3$ (df = 2; 90 % confidence interval $[-0.021, +0.035]$ K, wider than the equivalence margins $\delta = 0.010$ K and $\delta = 0.017$ K), reflecting the low power of an $N = 3$ test rather than a systematic effect. The per-member flag differences are themselves of the order of the ensemble internal variability and carry no consistent

the vertical-exchange state-handling rather than to the compilation environment. The smaller CTRL_B−REF signal (+0.027 K), however, is itself comparable to the per-member flag spread; we therefore base the implementation-choice conclusion on the CTRL_B−CTRL_A contrast, whose two executables share identical compilation flags, and treat CTRL_B−REF as the most flag-sensitive of the three pairings while CTRL_A−REF remains robust (signal an order of magnitude above the flag effect).

We contrast three pairwise differences: CTRL_A−REF (effect of zero-reinitialization relative to the legacy leak), CTRL_B−REF (effect of memory-preserving reinitialization relative to the legacy leak), and CTRL_B−CTRL_A (effect of the choice of fix implementation, holding the elimination of the leak fixed).

Each configuration is integrated as a three-member initial-condition ensemble (members $m = 1, 2, 3$), so that the spread among members measures the model's internal variability and the ensemble mean isolates the deterministic response to the code change. Members are generated by perturbing the spectral temperature field at the start of integration with deterministic pseudo-random shifts of amplitude $\varepsilon = 10^{-13}$ K, applied independently to every spectral coefficient. The amplitude is set at the double-precision round-off scale: at a typical tropospheric temperature of 300 K, the unit-in-the-last-place of the REAL∗8 representation (IEEE, 2019) is $300 \times 2^{-52} \approx 6.66 \times 10^{-14}$ K, so ε corresponds to approximately 1.5 ulp, guaranteed to flip at least one mantissa bit while remaining far below any physically meaningful temperature scale. This protocol follows the CESM Large Ensemble methodology of Kay et al. (2015), who initialise each ensemble member from a slightly perturbed atmospheric temperature field at the level of round-off error. The PRNG is initialised in repeatable mode via the Fortran 2018 `RANDOM_INIT(REPEATABLE=.TRUE.)` intrinsic, with member-distinct state obtained by deterministic warmup-discard scaled by member index, so that each $(\mathrm{REF}, \mathrm{CTRL\_A}, \mathrm{CTRL\_B}) \times$ (member) combination is exactly reproducible. The theoretical basis for ensemble spread emerging from

sign: the compilation-flag perturbation behaves as a change of initial conditions (Dörfler et al., 2022), not as a systematic bias, so the +0.067 K signal is not an artifact of the flag difference. The equivalence margin $\delta = 0.010$ K is set a priori to the inter-member standard deviation, the natural detectability threshold for ensemble-based consistency testing (Baker et al., 2015; Massonnet et al., 2020), with $\delta = 0.017$ K ($\frac{1}{4}$ of the signal) reported as a robustness bound.

such micro-perturbations is Lorenz (1969)'s analysis of deterministic chaos in flows with many scales of motion. Because the PRNG state depends only on the member index, REF, CTRL_A and CTRL_B of the same member start from the identical initial perturbation; the per-member difference is therefore paired both by member (shared perturbation) and by year (shared AMIP forcing). We pool the three members as approximately independent replications (exchangeable conditional on the shared AMIP forcing) of the same internal variability. This pooling is justified empirically by an inter-member consistency check—the between-member variance of the per-member climatological difference is statistically indistinguishable from the sampling variance expected under independent draws (the area-weighted median of the between-to-sampling variance ratio is 0.57 for CTRL_A−REF and 0.67 for CTRL_B−REF, against the median 0.70 of the null distribution, approximately $F(M-1, \sum_m (N_{\mathrm{eff},m}-1))$ with $M=3$; full quantiles are reported in Table S2)—and physically by the ergodicity of the AMIP atmosphere on the 30-year scale, where the influence of round-off initial perturbations on the climatology is negligible.

2.3 Statistical methodology

For each diagnostic field on the T42 Gaussian grid ($64 \times 128 = 8192$ cells), the pooled-paired difference between two configurations is tested for a non-zero mean at each cell. For member m and year t, the paired difference is $d_{m,t} = \mathrm{CTRL}_{m,t} - \mathrm{REF}_{m,t}$, formed on the 30 annual or per-season means. The paired construction is essential: empirical testing showed that the paired t-test yields approximately a 10^4-fold reduction in residual variance relative to an independent two-sample Welch test on this design (a t-statistic gain of ~ 7 on cells with $r \approx 0.99$), because the AMIP-shared forcing induces a between-configuration correlation $r \approx 0.99$ on most cells, and the residual variance after subtraction is several orders of magnitude smaller than the variance of either individual series.

The temporal autocorrelation of the residuals reduces the effective number of degrees of freedom; we apply the standard Trenberth (1984) correction (Trenberth, 1984), $N_{\mathrm{eff},m} = N\,(1 - r_{1,m})/(1 + r_{1,m})$, to each member's residual series $d_{m,\cdot}$ separately, where $r_{1,m}$ is its lag-1 autocorrelation and $N = 30$ (29 for DJF). We adopt the conservative cap $N_{\mathrm{eff},m} = \min\big(N,\, N(1 - r_{1,m})/(1 + r_{1,m})\big)$: a negative lag-1 autocorrelation on a 30-year record is more likely a sampling artefact than

genuine anti-persistence, so we do not credit a series with more independent samples than years (Zwiers & von Storch, 1995). The ensemble signal is the mean of the per-member climatological differences, $\Delta = M^{-1}\sum_m \bar{d}_m$ with $M = 3$; pooling the three members, its standard error is

$$\mathrm{SE}^2 = \frac{1}{M^2}\sum_{m=1}^{M}\frac{\sigma^2_{w,m}}{N_{\mathrm{eff},m}},$$

where $\sigma^2_{w,m}$ is the interannual variance of $d_{m,\cdot}$. The test statistic $t = \Delta/\mathrm{SE}$ is referred to a Student-t distribution with $\mathrm{df} = \sum_m (N_{\mathrm{eff},m} - 1)$ degrees of freedom, combining the within-member effective samples of the three members. This combined degrees-of-freedom expression is exact under equal within-member residual variances; for heteroscedastic members the Welch–Satterthwaite effective df is smaller and hence more conservative. Recomputing the headline contrasts with the Welch–Satterthwaite df reduces the across-cell median effective df for `tas` from 77 to 67 (CTRL_A−REF), yet changes the FDR-significant cell fraction by less than one percentage point (CTRL_A−REF: 41.56 % versus 40.77 %; CTRL_B−REF: 0.33 % versus 0.32 %), so the reported significance is insensitive to the equal-variance assumption.

With 8192 cells and a per-cell $\alpha = 0.05$, an uncorrected test would yield approximately 410 false-positive cells under the null. We control the false-discovery rate using the Benjamini–Hochberg procedure (Benjamini & Hochberg, 1995) at $q = 0.05$: the p-values are ranked and the cell of rank k is declared significant if $p_{(k)} \le q\,k/M_{\mathrm{tot}}$, where $M_{\mathrm{tot}} = 8192$ is the number of tests (distinct from the ensemble-member index m). When the test statistics are approximately multivariate normal with non-negative correlations—as holds for the spatially correlated climate fields analysed here—the correlation between adjacent grid cells induces positive regression dependence (PRDS), under which the Benjamini–Hochberg procedure controls the FDR at the nominal level (Benjamini & Yekutieli, 2001). We treat positive dependence as an assumption rather than a proven property: climate fields also carry negative teleconnection correlations at long range, but local spatial autocorrelation dominates the cell-to-cell dependence, a regime in which Benjamini–Hochberg remains a standard and well-behaved choice for spatial-field significance (Wilks, 2016); the arbitrary-dependence Benjamini–Yekutieli bound would scale the threshold by $\sum_{i=1}^{M_{\mathrm{tot}}} 1/i \approx 9.4$ and is not adopted here. All percentages

labelled "FDR-significant" in subsequent sections refer to the fraction of the 8192 cells passing this combined paired-t / Trenberth-correction / BH-FDR procedure.

For model-vs-observations comparison we report the cosine-of-latitude weighted mean bias at each cell and the cosine-of-latitude weighted pattern correlation, summarized in Taylor-diagram form following Taylor (2001). The effective-spatial-degrees-of-freedom methodology of Bretherton et al. (1999) informs the interpretation of pattern correlations but is not used to inflate confidence intervals on the bias estimates.

2.4 Observational datasets and regridding

Twelve (variable, observation) pairs are used in the model-vs-observation comparison of Section 5: 2 m air temperature (`tas`) against ERA5 (Hersbach et al., 2020); precipitation (`pr`) against ERA5 and against GPCP version 2.3 (Adler et al., 2018); mean sea-level pressure (`psl`) against ERA5; total cloud fraction (`clt`) against ERA5 and against ISCCP-H HGM v01r00 (Young et al., 2018); top-of-atmosphere upwelling shortwave (`rsut`) and longwave (`rlut`) radiation against CERES EBAF Ed. 4 (Loeb et al., 2018); zonal-mean air temperature (`ta`), specific humidity (`hus`), and zonal and meridional wind (`ua`, `va`) on pressure levels against ERA5 pressure-level fields. The observational reference window is 1979-01 to 2008-12 or the closest available overlap.

All observational datasets are regridded to the T42 model Gaussian grid using bicubic interpolation (`cdo remapbic`); ISCCP-H, distributed on a HEALPix-derived grid, requires the dedicated preprocessor described in the replication pipeline. Vertical interpolation is not applied: pressure-level diagnostics use the common pressure levels reported by the model output and the reanalysis.

2.5 Use of AI tools in manuscript preparation

The author used Claude (Anthropic, Inc.) as a writing assistant for copy-editing, structural revision of selected sections, and identification of internal inconsistencies during manuscript preparation. The AI tool was not used to generate scientific content, perform data analysis, design the experimental protocol, or produce figures; all scientific claims, numerical results, statistical procedures, ensemble

design, and figure generation were carried out by the author. The author is fully responsible for the manuscript content, including text portions that incorporate AI-assisted editorial input.

3 Bitwise Reproducibility Framework

The companion parallelization paper Vokhmintsev (2026a) establishes that the MGO T42L25 model, with the `VE_JRESET` fix in place and with deterministic spectral synthesis enforced in `COMSPE_PREJ_MOD`, `CVDDR_ACC_MOD` and `SPH_ACC_MOD`, achieves bitwise identity across $N \in \{1, 2, 4, 8, 12, 16, 32\}$ OpenMP threads on two distinct hardware platforms (AMD Zen 5 and Intel Ivy Bridge-EP). The reproducibility property reduces to three structural implementation conditions on the parallel kernel: (C1) ordered per-latitude reduction into the global spectral coefficients, (C2) isolation of all per-call working state, and (C3) disjoint per-thread writes into shared accumulators. Variant A and Variant C of the present paper each satisfy condition (C2), but differ in how the per-latitude state is initialized between calls. The formal theorem statement and an empirical verification of (C1)–(C3) for the MGO code are deposited in the Supplementary Information; the full proof, a detailed comparison with algorithmic approaches to bit-reproducibility, and a theoretical-applicability discussion for other spectral atmospheric general circulation models are presented in a companion methodological note in preparation for the numerical-software literature. Neither is required for the climate-impact analysis below.

4 Results: model-vs-model contrasts

We report three pairwise contrasts between the 30-year climatologies of REF, CTRL_A and CTRL_B: CTRL_A−REF, CTRL_B−REF and CTRL_B−CTRL_A. Statistical significance is assessed cell-by-cell on the T42 Gaussian grid using the pooled-paired t-test with Trenberth (1984) effective-degrees-of-freedom correction and Benjamini–Hochberg FDR control at $q = 0.05$ (Section 2.3).

4.1 Surface air temperature

Table 1 summarises the global-mean and area-weighted global-mean changes in 2 m air temperature (`tas`) for the three pairwise contrasts, by annual and seasonal

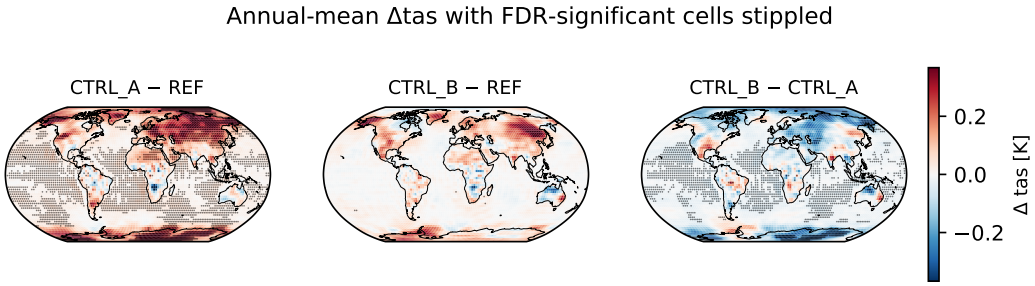

Figure 1. Annual-mean surface-air-temperature difference (Δ`tas`, K) for the three pairwise contrasts, as the three-member initial-condition ensemble mean. Stippling marks grid cells significant at the Benjamini–Hochberg FDR level ($q = 0.05$) under the pooled-paired t-test with the conservative N_{eff} cap (Section 2.3). The CTRL_A−REF warming is widespread and largely significant, the CTRL_B−REF response is weak, and the implementation-choice contrast CTRL_B−CTRL_A carries an extended significant signature of its own.

aggregation. The CTRL_A−REF response is a positive shift in the area-weighted annual mean of +0.0670 K, with 41.56 % of cells (3405 out of 8192) passing the BH-FDR criterion. The CTRL_B−REF response is substantially smaller, both in the area-weighted annual mean (+0.0274 K) and in the fraction of FDR-significant cells (0.33 %, 27 cells). The CTRL_B−CTRL_A contrast — which holds the elimination of the inter-J leak fixed and varies only the implementation of the reset — has an area-weighted annual mean of −0.0396 K and 20.34 % FDR-significant cells (1666 cells). In absolute area-weighted magnitude this implementation-choice signal exceeds the CTRL_B−REF physical-leak-elimination signal; in FDR-significant cell count it exceeds CTRL_B−REF by more than an order of magnitude. The spatial structure of the three contrasts is shown in Figure 1.

In all three contrasts the warm-season months carry larger signals than the boreal winter (DJF): the spring (MAM) and summer (JJA) seasons show the largest FDR-significant fractions, while DJF carries the smallest fraction of FDR-significant cells in every contrast. This is consistent with an interpretation in which the vertical-exchange parameterization is most active during the convective boundary-layer regime over Northern Hemisphere continents in the warm season, so that any artefact in the per-latitude initialization of the working arrays is amplified in the climatology of those seasons; the DJF season, in which mid- and high-latitude

Table 1. 30-year area-weighted mean change in 2 m air temperature (`tas`) for three pairwise contrasts, by annual and seasonal aggregation. Numbers in parentheses give the percentage of T42 cells (out of 8192) passing the paired-t / Trenberth / BH-FDR test at $q = 0.05$.

Season	CTRL_A−REF [K]	CTRL_B−REF [K]	CTRL_B−CTRL_A [K]
Annual	+0.0670 (41.56 %)	+0.0274 (0.33 %)	−0.0396 (20.34 %)
DJF	+0.0615 (3.38 %)	+0.0185 (0.00 %)	−0.0429 (2.21 %)
MAM	+0.0777 (12.61 %)	+0.0325 (0.37 %)	−0.0452 (7.70 %)
JJA	+0.0613 (13.81 %)	+0.0294 (1.17 %)	−0.0319 (9.74 %)
SON	+0.0697 (10.74 %)	+0.0296 (0.00 %)	−0.0401 (4.93 %)

Northern-Hemisphere variability is dominated by baroclinic activity with a smaller vertical-exchange contribution, carries the weakest signal.

4.2 Auxiliary surface and column-integrated fields

For the annual mean we report three auxiliary fields: total cloud fraction (`clt`), mean sea-level pressure (`psl`), and precipitation (`pr`). The corresponding numbers are summarised in Table 2.

Table 2. 30-year area-weighted annual-mean change for the auxiliary fields. The same FDR test as Table 1 is applied. Precipitation differences in area-weighted global mean are below 10^{-4} mm d^{-1} in all three contrasts; the FDR-significant cell percentage reflects regional rearrangement that cancels in the global integral.

Field [unit]	CTRL_A−REF	CTRL_B−REF	CTRL_B−CTRL_A
`clt` [%]	−0.4016 (19.63 %)	−0.1641 (8.31 %)	+0.2375 (4.10 %)
`psl` [Pa]	+0.0119 (0.00 %)	−0.3659 (0.37 %)	−0.3778 (0.00 %)
`pr` [mm d^{-1}]	$< 10^{-4}$ (0.02 %)	$< 10^{-4}$ (0.00 %)	$< 10^{-4}$ (0.00 %)

The cloud-fraction response shows the same leading ordering as `tas`: the zero-reinitialization fix (CTRL_A−REF) produces the largest shift, both in global mean (−0.40 %) and in FDR-significant cell count (19.63 %). For the implementation-

choice contrast (CTRL_B−CTRL_A) the area-weighted shift (+0.24 %) exceeds that of the physical CTRL_B−REF contrast (−0.16 %), though with a smaller FDR-significant fraction. The mean sea-level pressure response is dominated by regional dipoles which largely cancel in the global integral. The precipitation response in area-weighted global mean is at the level of numerical noise but exhibits a regional FDR pattern consistent with rearrangement of convective rainfall rather than a net change in the global hydrological cycle.

4.3 Implementation choice exceeds physical-leak elimination

The central model-vs-model observation of this paper is contained in Tables 1 and 2. The CTRL_B−CTRL_A contrast, which varies only the implementation of the vertical-exchange reset (zero versus per-J snapshot/restore) and not the elimination of the inter-J leak itself, produces for `tas` a climate response that exceeds the physical CTRL_B−REF contrast in both area-weighted magnitude ($|\Delta_{\mathrm{aw}}| = 0.0396$ K versus 0.0274 K) and FDR-significant cell count (20.34 % versus 0.33 %). For `clt` the implementation-choice contrast exceeds the physical contrast in area-weighted magnitude (0.2375 % versus 0.1641 %) while carrying a smaller FDR-significant fraction (4.10 % versus 8.31 %). The qualitative statement is robust across both fields: holding the elimination of the leak fixed, the choice of how to reset the working arrays carries an FDR-significant climate signature comparable to, and for `tas` substantially larger than, the removal of the leak itself.

4.3.0.1 Ensemble basis. All numbers in Tables 1 and 2 are pooled-paired estimates over the three-member initial-condition ensemble (Section 2.3). The inter-member consistency check confirms that the between-member spread is consistent with sampling, so the three members are pooled as independent replications; the reported significance therefore reflects both the within-member temporal sampling and the between-member initial-condition spread.

5 Results: model-vs-observations

5.1 Annual scorecard

Table 3 reports the area-weighted bias against observations for the three configurations across twelve (variable, observation) pairs at annual mean. Each row gives

the absolute bias $|\overline{\text{model}} - \overline{\text{obs}}|$ for REF, CTRL_A and CTRL_B, the percentage reduction (negative values indicate degradation) of each fix relative to REF, and the winning configuration.

Table 3. Annual-mean area-weighted absolute bias against observations for twelve (variable, observation) pairs. "A red. %" and "B red. %" give the percentage reduction of |bias| in CTRL_A and CTRL_B relative to REF; negative values indicate degradation. Winner denotes the lower-bias configuration between CTRL_A and CTRL_B; REF is the uncorrected baseline and does not compete. Aggregating across the twelve pairs, CTRL_A wins four and CTRL_B wins eight. Reduction percentages are computed from full-precision biases and may not be exactly reproducible from the rounded |bias| columns.

Var	Obs	|REF|	|CTRL_A|	|CTRL_B|	A red. %	B red. %	Winner
`tas`	ERA5	0.1837	0.1167	0.1563	+36.5	+14.9	CTRL_A
`pr`	ERA5	0.2196	0.2299	0.2197	−4.7	−0.1	CTRL_B
`pr`	GPCP	0.4225	0.4328	0.4227	−2.4	−0.0	CTRL_B
`psl`	ERA5	16.03	16.01	16.39	+0.1	−2.3	CTRL_A
`clt`	ERA5	13.10	13.50	13.26	−3.1	−1.3	CTRL_B
`clt`	ISCCP	16.87	17.27	17.03	−2.4	−1.0	CTRL_B
`rsut`	CERES	2.199	3.349	3.061	−52.3	−39.2	CTRL_B
`rlut`	CERES	6.433	6.603	6.531	−2.6	−1.5	CTRL_B
`ta`	ERA5p	0.1444	0.1226	0.1011	+15.1	+30.0	CTRL_B
`hus`	ERA5p	5.45e-5	4.79e-5	5.25e-5	+12.1	+3.7	CTRL_A
`ua`	ERA5p	1.147	1.102	1.131	+4.0	+1.4	CTRL_A
`va`	ERA5p	0.00714	0.00723	0.00701	−1.3	+1.8	CTRL_B

Aggregating across the twelve pairs, CTRL_A is the lower-bias configuration in four pairs (`tas`, `psl`, `hus`, `ua`) and CTRL_B in eight pairs (`pr` against both `ERA5` and `GPCP`, `clt` against both `ERA5` and `ISCCP`, `rsut`, `rlut`, `ta`, `va`). The aggregate score does not identify a configuration that uniformly improves the simulated climate against observations: the trade-off between the two fixes is field-dependent, with CTRL_A favoured on near-surface and lower-tropospheric fields (`tas`, `psl`,

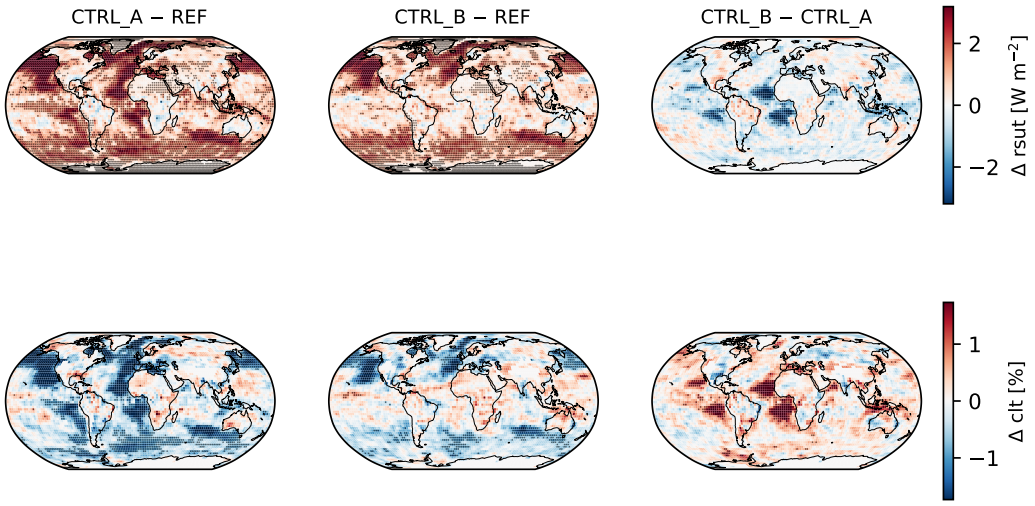

Figure 2. As Figure 1 but for top-of-atmosphere upwelling shortwave radiation (Δ`rsut`, $\mathrm{W\,m^{-2}}$; top row) and total cloud fraction (Δ`clt`, %; bottom row), the two diagnostics that both fixes degrade relative to the legacy code. Stippling marks BH-FDR-significant cells ($q = 0.05$).

`hus`, `ua`) and CTRL_B favoured on column-integrated, radiative, free-tropospheric thermodynamic, and meridional-wind fields.

5.2 Both fixes increase radiative and cloud biases

The most consequential entry in Table 3 for the interpretation of the experiment is the row for the top-of-atmosphere upwelling shortwave radiation `rsut` against CERES EBAF. The REF bias is $-2.20\ \mathrm{W\,m^{-2}}$ (the model underestimates the global mean outgoing shortwave by $2.2\ \mathrm{W\,m^{-2}}$ relative to CERES), the CTRL_A bias is $-3.35\ \mathrm{W\,m^{-2}}$, and the CTRL_B bias is $-3.06\ \mathrm{W\,m^{-2}}$. Both fixes therefore enlarge the absolute shortwave bias relative to the legacy code, by 52 % and 39 % respectively. The same direction is found for outgoing longwave `rlut` ($+6.43\ \mathrm{W\,m^{-2}}$ REF, +6.60 CTRL_A, +6.53 CTRL_B; degradations of 2.6 % and 1.5 %), for total cloud fraction against ERA5 (−13.10 % REF, −13.50 % CTRL_A, −13.26 % CTRL_B; degradations of 3.1 % and 1.3 %), and for total cloud fraction against ISCCP (−16.87 %, −17.27 %, −17.03 %; degradations of 2.4 % and 1.0 %).

The pattern is consistent across all four (variable, observation) pairs in the radiative-and-cloud group: both implementations of the vertical-exchange fix increase the absolute bias relative to the legacy code, and the zero-reinitialization variant (CTRL_A) degrades the bias more than the memory-preserving variant (CTRL_B). The same group of fields, taken together, contains the largest single observational degradation in the experiment (`rsut` −52 % in CTRL_A).

We note that surface air temperature against ERA5 follows the opposite pattern: CTRL_A reduces the cold bias by 37 % and CTRL_B by 15 %, both relative to REF. The full `tas`-improvement-with-`rsut`-degradation pattern is the observational fingerprint that motivates the implicit-tuning interpretation discussed in Section 6.

5.3 Taylor-diagram interpretation: amplitude shift, not spatial

The pattern correlations of `tas` against ERA5 (annual mean and four seasons) lie in the narrow range 0.9886 to 0.9921 across all three configurations REF, CTRL_A and CTRL_B (full per-season values are tabulated in the Supporting Information). The maximum cross-configuration spread in any given season is 0.0001 in the correlation coefficient. The same insensitivity of the pattern correlation to the choice of configuration is found for the auxiliary fields: REF, CTRL_A and CTRL_B differ on the Taylor diagram (Figure 3) by displacement along the standard-deviation axis and by translation of the mean bias, but they are essentially indistinguishable in their angular position (pattern correlation with the observational reference).

The geophysical interpretation is that neither implementation of `VE_JRESET` corrects the spatial signature of the model bias relative to observations: the well-documented cold bias of the MGO T42L25 over Northern Hemisphere high latitudes, the wet bias of the tropical convergence zones against GPCP, and the negative cloud-fraction bias against ERA5 and ISCCP-H all persist in identical spatial patterns under both fixes. What changes between configurations is the amplitude of the bias, not its geography. This diagnosis sharpens the implicit-tuning hypothesis of Section 6: a structural code modification that rebalances amplitudes without correcting patterns is the expected signature of a perturbation to a tuned parameter set, rather than of a correction to a missing physical process.

5.3.0.1 Ensemble basis of the scorecard. The model-vs-observation scorecard of Table 3 is computed from the three-member initial-condition ensemble-mean 30-year climatology of each configuration, consistent with the pooled-paired estimates of Section 4. Bias differences between configurations smaller than the inter-member ensemble spread (of order 0.01 K for global-mean `tas`) are reported for completeness but should not be over-interpreted as robust improvements.

6 Discussion

The two central empirical observations of Sections 4–5 are (i) that the choice of implementation of the vertical-exchange reset produces an FDR-significant climate signature comparable in magnitude to the elimination of the inter-J leak itself, and (ii) that both implementations enlarge the radiation and cloud biases of the model against observations while reducing the surface-temperature bias. Both observations are consistent with the hypothesis that the legacy REF configuration was implicitly tuned against the leaky baseline—that is, that other elements of the parameter set were calibrated against observations in the presence of the state-leakage and partially compensated for it—and that eliminating the leakage in either of the two implementations displaces the model from that compensated optimum (Mauritsen et al., 2012; Hourdin et al., 2017; Mauritsen et al., 2019; Schmidt et al., 2017). We emphasise that this is an observation-consistent hypothesis rather than a proven proposition: distinguishing it from alternative mechanisms (for example, residual numerical nonlinearities specific to the boundary-layer or cloud-radiation parameterizations at the present horizontal resolution) requires a dedicated re-tuning experiment that is not part of the present work.

6.1 Implicit tuning in the climate-model development literature

Implicit tuning is an established concept in the climate-model development literature. Mauritsen et al. (2012) formalized the practice of tuning a coupled global climate model and explicitly described how adjustments to one parameter are commonly compensated by adjustments to others in order to preserve top-of-atmosphere radiative balance, producing parameter sets whose individual values are not separately identifiable from observations. Hourdin et al. (2017) systematized this practice across the major modelling centres and argued that the tuning process

itself constitutes a scientific activity that should be documented alongside model code. Earlier single-centre case studies documented the same compensation dynamics: Pope et al. (2000) reported the systematic re-tuning required when the Hadley Centre HadAM3 physics suite was changed, and Williamson (2008) demonstrated parameter-dependent convergence of cloud and radiation fields with resolution in aqua-planet simulations using CAM3. Schmidt et al. (2017) surveyed six US modelling centres and reported a core commonality of tuning approaches across institutions while also documenting significant differences in specific practices (use of forecast initialization, transient warming targets, and choice of preindustrial vs. present-day TOA balance); and Mauritsen et al. (2019) documented a specific instance of compensating coding errors in cloud, convection, and turbulence parameterizations, accompanied by parameter retuning during the development of MPI-ESM1.2. Golaz et al. (2013) traced cloud-tuning choices in GFDL CM3 to sizeable impacts on simulated twentieth-century surface-temperature evolution, and Voldoire et al. (2019) described the development and evaluation of CNRM-CM6-1 for CMIP6 DECK, including parameter choices that significantly affect the equilibrium climate sensitivity. Bender (2008) demonstrated quantitatively that GCM tuning choices alone can shift equilibrium climate sensitivity by appreciable amounts; community-organized evaluation frameworks—the CMIP5/CMIP3 cloud comparison of Lauer and Hamilton (2013) and the CFMIP-3 cloud-feedback protocol of Webb et al. (2017)—formalize the multi-model verification that single-centre tuning alone cannot provide. What appears to be absent from this literature is a quantitative *paired* case study in which a single identified bug is fixed by two alternative implementations, with both contrasted against a shared legacy baseline under identical statistical treatment. The present work is offered as one such case.

6.2 Physical mechanism for the warm-season concentration of the signal

The warm-season concentration of the FDR-significant response—largest in MAM and JJA and smallest in DJF in every contrast (Table 1), as noted in Section 4.1—is consistent with a physically plausible mechanism in the vertical-exchange parameterization itself. Over Northern Hemisphere continents in boreal summer the convective planetary boundary layer extends to 1–3 km and is actively

mixed at every physics time step; the vertical-exchange working arrays whose initialization is varied between configurations would on this account be re-engaged on every column. In boreal winter the Northern Hemisphere boundary layer is shallow, stably stratified, and dominated by baroclinic-eddy heat transport, so the vertical-exchange contribution to the climatological tendency would be comparatively small. The numbers in Table 1 are consistent with this picture in the spatial extent of the signal rather than its area-weighted amplitude: the warm-season fractions of FDR-significant cells (MAM 12.6 %, JJA 13.8 %, SON 10.7 % for CTRL_A−REF) are three to four times the DJF fraction (3.4 %), while the area-weighted seasonal amplitudes show no clean ordering (CTRL_A−REF JJA +0.0613 K and DJF +0.0615 K are nearly equal, with MAM +0.0777 K the largest). We emphasise that this interpretation is post hoc: the ratios are observed and then rationalised by an appeal to boundary-layer physics, rather than being predicted ex ante from the parameterization parameters. An ex-ante derivation of the expected JJA/DJF ratio from the closure parameters of the Mellor–Yamada PBL and the seasonal cycle of continental convective engagement is a sharper test of the mechanism and is left to future work.

6.3 Choice of fix implementation as a methodological finding

The central novelty of this paper is the CTRL_B−CTRL_A contrast of Section 4.3: holding the elimination of the inter-J leak fixed, the choice between a physically motivated implementation (CTRL_B, which preserves the per-latitude previous-time-step state) and an algorithmically motivated one (CTRL_A, which zeroes the working arrays) of that same fix paradigm produces a statistically significant climate signature (20.34 % FDR-significant cells on annual `tas`, 1666 of 8192) that, on `tas`, exceeds the CTRL_B−REF elimination of the leak in both area-weighted magnitude and FDR-significant extent.

CTRL_A is not a straw-man comparator. Zero-reinitialization is the default outcome of a thread-safety audit that removes the inter-latitude leak without a physics review of each `SAVE` array, and is therefore precisely the fix a modernization effort would adopt in the absence of the present analysis. The finding is thus that a physically defensible and an algorithmically defensible repair of the same bug—both reasonable choices for a maintainer of legacy code whose original developers cannot be consulted—diverge at climate scale, a sharper statement than the truism that

arbitrary code perturbations produce different results. The implication is methodological rather than narrowly diagnostic. In the legacy-GCM bug-fix reports we have surveyed, the fix is typically treated as a unique decision (one fix per bug, reported as "the" fix) and its impact is quantified against a single baseline. The demonstration here that a physically defensible and an algorithmically defensible implementation of the same fix paradigm produce climate-scale differences of their own forces a re-evaluation of that reporting practice for legacy-code modernization, particularly in codes whose original developers cannot be consulted on implementation intent. To the author's knowledge, a paired quantitative comparison of two alternative implementations of the same physical fix does not appear to have been reported in the climate-model bug-fix literature.

6.4 Limitations

Six limitations qualify the conclusions drawn above. *(i)* Each configuration is represented by a three-member initial-condition ensemble. The inter-member consistency check confirms that the between-member spread is sampling-dominated, which supports pooling the members as approximately independent replications; nonetheless, three members provide only a limited estimate of internal variability, and the ensemble establishes the robustness of the implementation-choice signal without isolating its mechanism—the causal attribution to implicit tuning would require the re-tuning experiment of item (iii). *(ii)* The analysis is restricted to one model. The argument that the inter-J state-leakage class is generic to legacy F77 GCMs that rely on `SAVE`+ `THREADPRIVATE` working arrays under OpenMP parallelization is theoretical rather than empirical; replication on a second legacy spectral GCM such as IFS or a pre-modernization release of ECHAM would substantively strengthen the generalization claim. *(iii)* No dedicated re-tuning experiment is performed. The implicit-tuning interpretation of Section 5.2 remains an observation-consistent hypothesis rather than a proven proposition; the direct verification—re-tuning a CTRL_B configuration against observations to restore the radiation and cloud agreement, and then comparing the re-tuned configuration to REF—would require a further 30-year run and parameter-calibration expertise specific to the MGO parameterization suite, and is deferred to follow-up work. *(iv)* The implementation contrast is conducted at the level of the full 25-array working state of the vertical-exchange

routine; a sensitivity-to-subset experiment, in which only a subset of the 25 arrays is treated under each variant, has not been performed and may reveal that the climate sensitivity is concentrated in a few arrays rather than evenly distributed across the working state. *(v)* The model configuration is methodologically bounded. The horizontal resolution T42L25 ($\approx$ 2.8°) and the AMIP-style prescribed-SST forcing are deliberate scope choices that isolate the parallelization-induced implementation-choice signal from confounding sources: at higher horizontal resolutions (T63L25 and T106L25 are available in our codebase) and under interactive ocean coupling, additional artifacts—memory-bandwidth limits, NUMA effects, and ocean–atmosphere feedback loops—would obscure the attribution to vertical-exchange state handling. Whether the same class of implicit-tuning interaction arises in fully-coupled high-resolution CMIP6 or CMIP7 models, where boundary-layer treatment, ocean–atmosphere coupling, and horizontal resolution all differ qualitatively from the present configuration, is an open question to be addressed in dedicated companion papers at T63L25 and T106L25 currently in preparation. A related caveat applies to the top-of-atmosphere energy balance: under prescribed-SST AMIP forcing the TOA radiative imbalance is a diagnostic indicator only and does not feed back on surface temperature, whereas in a fully-coupled configuration the $\sim$ 1 $\mathrm{W\,m^{-2}}$ shortwave degradation would drive a surface-temperature drift—the very pathway through which the implicit-tuning compensation identified here would manifest. *(vi)* The implicit-tuning interpretation is not uniquely distinguishable from a slow-equilibration alternative in the present 30-year design. Even under prescribed-SST and prescribed-ozone AMIP forcing, the atmospheric and land-surface systems carry internal adjustment timescales—from soil-moisture memory of months to multi-metre soil-thermal and stratospheric mass-exchange memory of years (Seneviratne et al., 2010; Holton et al., 1995)—that can extend beyond the 30-year integration window. The CTRL_A versus CTRL_B contrast might therefore reflect, in part, different equilibration trajectories from a shared physical attractor rather than a stable shift in the implicit-tuning of the radiation-cloud balance. Within the 30-year window itself the pairwise global-mean Δ`tas` shows no significant trend (Figure 4; $|\mathrm{trend}| < 0.013$ $\mathrm{K\,decade^{-1}}$ for all three contrasts), which is consistent with a stable shift but does not exclude slower adjustment beyond the integration length. Empirically distinguishing the two requires either a substantially longer integration (60–100

years per configuration) to verify that the contrast persists rather than decays, or a direct re-tuning experiment (item iii above). Both options are computationally non-trivial at single-investigator scale; the present results should therefore be read as a case study of the implementation-choice signal within a finite-window AMIP framework, with the slow-equilibration alternative explicitly acknowledged as an unresolved possibility.

7 Conclusions

The tri-experiment study reported above supports four takeaways.

1. *Inter-step state-leakage through `SAVE`-attribute working arrays is plausibly a generic class of bugs in legacy Fortran 77 atmospheric GCMs*, although the present evidence is from a single model (Section 6.4). The class is activated by the addition of OpenMP parallelization without a corresponding audit of all `SAVE`+`THREADPRIVATE` working state in the physics parameterizations. We recommend that a structural audit of such arrays be a standard step in the modernization of legacy atmospheric codes.
2. *The choice of implementation of a single physical fix is itself a climate-scale design decision, not a cosmetic refactoring choice.* A physically motivated (CTRL_B, per-latitude snapshot/restore) and an algorithmically motivated (CTRL_A, zero-reinitialization) implementation of the same fix paradigm produce statistically significant differences in 30-year climatology (20.34 % FDR-significant cells on annual `tas`, 1666 of 8192). Bug-fix reporting in legacy-GCM development should accordingly include explicit justification of the implementation chosen, rather than presenting the fix as if unique.
3. *An implicit-tuning interaction is quantified in one empirical case.* Both alternative implementations of the vertical-exchange fix worsen the agreement of the simulated radiation and cloud fields with observations (Section 5.2; Table 3), in a manner consistent with the hypothesis that the legacy REF configuration was implicitly tuned against the leaky baseline. A direct re-tuning experiment, in which a CTRL_B configuration is re-calibrated against observations to restore the radiation balance and then contrasted against REF, is deferred to follow-up work as the natural verification of this hypothesis.

4. *The tri-experiment design (REF plus two alternative fixes) is recommended as a methodological template for future legacy-GCM bug-fix studies.* The design separates the physical-leak-elimination effect from the implementation-choice effect by construction; either effect in isolation can be assessed against a shared baseline.

Taken together, the bit-reproducibility audit of the companion parallelization paper and the implicit-tuning quantification of the present work provide a methodological foundation for the credible reporting of model-refactoring outcomes. This pairing is of particular value for legacy codes that lack extensive automated test coverage, where the absence of a regression suite makes the distinction between a structural fix and an implementation choice otherwise difficult to assess.

The bit-identity theorem of the Supporting Information and the tri-experiment design developed here are resolution-agnostic and do not depend on the choice between AMIP-style prescribed forcing and interactive ocean coupling; they constitute a reusable methodological framework for subsequent evaluations of the same legacy codebase at T63L25 and T106L25, where new parallelization or numerical artifacts may emerge at higher computational load.

Open Research Statement

The MGO atmospheric general circulation model is proprietary legacy code maintained by the Voeikov Main Geophysical Observatory (Saint Petersburg, Russia); its underlying source code is not publicly redistributable. The thread-safety modifications referenced in this paper (`VE_JRESET` in the vertical-exchange kernel and the deterministic-reduction modules `COMSPE_PREJ_MOD`, `CVDDR_ACC_MOD`, `SPH_ACC_MOD`) constitute new code authored by the present author and are publicly available as a diff/patch package in the companion replication archive (Vokhmintsev, 2026c), which also contains MD5 checksum tables for thread-count verification, OpenMP performance measurements, and reproducibility scripts for the companion parallelization paper. The derived statistical products supporting the present manuscript (paired difference fields with Benjamini–Hochberg FDR-significance masks, model-vs-observation validation Taylor statistics against ERA5, CERES EBAF, GPCP, and ISCCP-H, inter-member consistency F-ratio fields,

annual global-mean diagnostics) together with the analysis scripts that reproduce all manuscript tables and figures are archived in the Paper 2 replication package (Vokhmintsev, 2026b). Observational datasets (ERA5, CERES EBAF, GPCP, ISCCP-H) are obtained through public APIs; versions and access details are listed in the `PROVENANCE.md` file of the replication package. Boundary conditions (monthly SST/sea-ice forcing for the AMIP-style integration period 1979–2008) follow the CFSR/CMIPMOD protocol and are documented in the same file. Direct access to the unmodified MGO source code is not at the present author's disposal to grant. Because this manuscript is submitted as independent research with no current institutional affiliation, for verification questions that cannot be resolved from the deposited replication materials, the author will provide upon reviewer request targeted excerpts of the author's own modifications, structural diagrams of the relevant code paths, or written walk-throughs.

Conflict of Interest disclosure

The author was previously employed at the Voeikov Main Geophysical Observatory (Saint Petersburg, Russia) for a 2.5-year period during which the parallelization of the MGO atmospheric general circulation model was initiated but not completed; this employment concluded in July 2025. The substantive work reported in the present manuscript— including the discovery of the inter-latitude state leakage in the vertical-exchange parameterization (`VE_JRESET`), the formal bit-reproducibility theorem, the three-member tri-experiment ensemble design (REF / CTRL_A / CTRL_B), the paired statistical framework, and the entire climate-impact analysis—was completed over the subsequent year as an independent, self-directed effort on personal computational resources, without institutional affiliation or external funding. The author has no current affiliation with, or financial interest in, the Voeikov Main Geophysical Observatory or any related institution. The author holds one issued Rospatent computer-program registration covering the structural repair, the deterministic-reduction modules, and the analysis pipeline reported here, and has two related Rospatent patent applications under examination on the parallel-reduction and thread-safety methodology; these are derivative works that do not cover the proprietary MGO model itself. The author declares no other conflicts of interest for this manuscript.

Acknowledgments

The author thanks V. A. Matyugin, A. V. Baydin, P. V. Sporyshev, and I. M. Shkolnik of the Department of Dynamic Meteorology and Climatology at the Voeikov Main Geophysical Observatory (St. Petersburg) for the development, maintenance, and scientific stewardship of the MGO atmospheric general circulation model on which the present work builds; the structural modifications documented here (`VE_JRESET`, `VE_MEM_MOD`, and the deterministic-reduction modules) and all subsequent analyses are the present author's independent contributions. The companion parallelization study Vokhmintsev (2026a) established the bit-reproducibility properties of the corrected code that underpin the experimental contrast reported here. The observational datasets used in Section 5 are made openly available by ECMWF (ERA5), NASA (CERES EBAF and ISCCP-H), and NOAA/GPCP; the author gratefully acknowledges these contributions to the community record of atmospheric observations. The analysis pipelines rely on the open-source scientific Python stack (xarray, numpy, scipy, matplotlib) and the Climate Data Operators (CDO); the maintainers of these projects are thanked. Computational resources for the 30-year integrations were self-funded.

References

Adler, R. F., Sapiano, M. R. P., Huffman, G. J., Wang, J.-J., Gu, G., Bolvin, D., ... Shin, D.-B. (2018). The Global Precipitation Climatology Project (GPCP) Monthly Analysis (New Version 2.3) and a review of 2017 global precipitation. *Atmosphere*, *9*(4), 138. doi: 10.3390/atmos9040138

Baker, A. H., Hammerling, D. M., Levy, M. N., Xu, H., Dennis, J. M., Eaton, B. E., ... Williamson, D. (2015). A new ensemble-based consistency test for the Community Earth System Model (pyCECT v1.0). *Geoscientific Model Development*, *8*(9), 2829–2840. doi: 10.5194/gmd-8-2829-2015

Bechtold, P., Köhler, M., Jung, T., Doblas-Reyes, F., Leutbecher, M., Rodwell, M. J., ... Balsamo, G. (2008). Advances in simulating atmospheric variability with the ECMWF model: From synoptic to decadal time-scales. *Quarterly Journal of the Royal Meteorological Society*, *134*(634), 1337–1351. doi: 10.1002/qj.289

Bender, F. A.-M. (2008). A note on the effect of GCM tuning on climate sensitiv-

ity. *Environmental Research Letters*, *3*(1), 014001. doi: 10.1088/1748-9326/3/1/014001

Benjamini, Y., & Hochberg, Y. (1995). Controlling the false discovery rate: a practical and powerful approach to multiple testing. *Journal of the Royal Statistical Society: Series B*, *57*(1), 289–300. doi: 10.1111/j.2517-6161.1995.tb02031.x

Benjamini, Y., & Yekutieli, D. (2001). The control of the false discovery rate in multiple testing under dependency. *The Annals of Statistics*, *29*(4), 1165–1188. doi: 10.1214/aos/1013699998

Bourke, W. (1974). A multi-level spectral model. I. Formulation and hemispheric integrations. *Monthly Weather Review*, *102*(10), 687–701. doi: 10.1175/1520-0493(1974)102⟨0687:AMLSMI⟩2.0.CO;2

Bretherton, C. S., Widmann, M., Dymnikov, V. P., Wallace, J. M., & Bladé, I. (1999). The effective number of spatial degrees of freedom of a time-varying field. *Journal of Climate*, *12*(7), 1990–2009. doi: 10.1175/1520-0442(1999)012⟨1990:TENOSD⟩2.0.CO;2

Bulgakov, K. Y., Meleshko, V. P., & Shneerov, B. E. (2008). On sensitivity of equilibrium climate to CO_2 doubling. In V. M. Kattsov & V. P. Meleshko (Eds.), *Proceedings of the voeikov main geophysical observatory* (Vol. 558, pp. 3–27). Saint Petersburg, Russia: Voeikov Main Geophysical Observatory. (In Russian. Equilibrium climate sensitivity studies using MGO T42L25 configuration)

Dörfler, B., Ageev, A., Ayet, A., Hettrich, S., Kohl, A., Leutbecher, M., & Wedi, N. (2022). An ensemble-based statistical methodology to detect differences in weather and climate model executables. *Geoscientific Model Development*, *15*, 3183–3203. doi: 10.5194/gmd-15-3183-2022

Eyring, V., Bony, S., Meehl, G. A., Senior, C. A., Stevens, B., Stouffer, R. J., & Taylor, K. E. (2016). Overview of the Coupled Model Intercomparison Project Phase 6 (CMIP6) experimental design and organization. *Geoscientific Model Development*, *9*(5), 1937–1958. doi: 10.5194/gmd-9-1937-2016

Gates, W. L., Boyle, J. S., Covey, C., Dease, C. G., Doutriaux, C. M., Drach, R. S., ... Williams, D. N. (1999). An overview of the results of the Atmospheric Model Intercomparison Project (AMIP I). *Bulletin of the American Meteorological Society*, *80*(1), 29–55. doi: 10.1175/1520-0477(1999)080⟨0029:AOOTRO⟩2.0.CO;2

Golaz, J.-C., Horowitz, L. W., & Levy, H. (2013). Cloud tuning in a coupled climate model: Impact on 20th century warming. *Geophysical Research Letters*, *40*(10), 2246–2251. doi: 10.1002/grl.50232

Hersbach, H., Bell, B., Berrisford, P., Hirahara, S., Horányi, A., Muñoz-Sabater, J., et al. (2020). The ERA5 global reanalysis. *Quarterly Journal of the Royal Meteorological Society*, *146*(730), 1999–2049. doi: 10.1002/qj.3803

Holton, J. R., Haynes, P. H., McIntyre, M. E., Douglass, A. R., Rood, R. B., & Pfister, L. (1995). Stratosphere-troposphere exchange. *Reviews of Geophysics*, *33*(4), 403–439. doi: 10.1029/95RG02097

Holtslag, A. A. M., & Boville, B. A. (1993). Local versus nonlocal boundary-layer diffusion in a global climate model. *Journal of Climate*, *6*(10), 1825–1842. doi: 10.1175/1520-0442(1993)006⟨1825:LVNBLD⟩2.0.CO;2

Hourdin, F., Mauritsen, T., Gettelman, A., Golaz, J.-C., Balaji, V., Duan, Q., ... Williamson, D. (2017). The art and science of climate model tuning. *Bulletin of the American Meteorological Society*, *98*(3), 589–602. doi: 10.1175/BAMS-D-15-00135.1

IEEE. (2019). *IEEE standard for floating-point arithmetic.* doi: 10.1109/IEEESTD.2019.8766229

Kay, J. E., Deser, C., Phillips, A., Mai, A., Hannay, C., Strand, G., ... Vertenstein, M. (2015). The Community Earth System Model (CESM) Large Ensemble Project: A community resource for studying climate change in the presence of internal climate variability. *Bulletin of the American Meteorological Society*, *96*(8), 1333–1349. doi: 10.1175/BAMS-D-13-00255.1

Lauer, A., & Hamilton, K. (2013). Simulating clouds with global climate models: A comparison of CMIP5 results with CMIP3 and satellite data. *Journal of Climate*, *26*(11), 3823–3845. doi: 10.1175/JCLI-D-12-00451.1

Loeb, N. G., Doelling, D. R., Wang, H., Su, W., Nguyen, C., Corbett, J. G., ... Kato, S. (2018). Clouds and the Earth's Radiant Energy System (CERES) Energy Balanced and Filled (EBAF) top-of-atmosphere (TOA) edition-4.0 data product. *Journal of Climate*, *31*(2), 895–918. doi: 10.1175/JCLI-D-17-0208.1

Lorenz, E. N. (1969). The predictability of a flow which possesses many scales of motion. *Tellus*, *21*(3), 289–307. doi: 10.3402/tellusa.v21i3.10086

Massonnet, F., Ménégoz, M., Acosta, M., Yepes-Arbós, X., Exarchou, E., & Doblas-

Reyes, F. J. (2020). Replicability of the EC-Earth3 Earth system model under a change in computing environment. *Geoscientific Model Development*, *13*(3), 1165–1178. doi: 10.5194/gmd-13-1165-2020

Mauritsen, T., Bader, J., Becker, T., Behrens, J., Bittner, M., Brokopf, R., ... Roeckner, E. (2019). Developments in the MPI-M Earth System Model version 1.2 (MPI-ESM1.2) and its response to increasing CO_2. *Journal of Advances in Modeling Earth Systems*, *11*(4), 998–1038. doi: 10.1029/2018MS001400

Mauritsen, T., Stevens, B., Roeckner, E., Crueger, T., Esch, M., Giorgetta, M., ... Tomassini, L. (2012). Tuning the climate of a global model. *Journal of Advances in Modeling Earth Systems*, *4*(3), M00A01. doi: 10.1029/2012MS000154

Meleshko, V. P., Matyugin, V. A., Sporyshev, P. V., Pavlova, T. V., Govorkova, V. A., Shkolnik, I. M., & Baidin, A. V. (2014). MGO general circulation model (version MGO-03 T63L25). *Proceedings of the Voeikov Main Geophysical Observatory*, *571*, 5–87. (In Russian. Describes both T63L25 (climate) and T42L25 (coupled ocean–atmosphere–cryosphere) production configurations)

Mellor, G. L., & Yamada, T. (1974). A hierarchy of turbulence closure models for planetary boundary layers. *Journal of the Atmospheric Sciences*, *31*(7), 1791–1806. doi: 10.1175/1520-0469(1974)031⟨1791:AHOTCM⟩2.0.CO;2

Mellor, G. L., & Yamada, T. (1982). Development of a turbulence closure model for geophysical fluid problems. *Reviews of Geophysics*, *20*(4), 851–875. doi: 10.1029/RG020i004p00851

Pope, V. D., Gallani, M. L., Rowntree, P. R., & Stratton, R. A. (2000). The impact of new physical parametrizations in the Hadley Centre climate model: HadAM3. *Climate Dynamics*, *16*(2-3), 123–146. doi: 10.1007/s003820050009

Rosinski, J. M., & Williamson, D. L. (1997). The accumulation of rounding errors and port validation for global atmospheric models. *SIAM Journal on Scientific Computing*, *18*(2), 552–564. doi: 10.1137/S1064827594275534

Schär, C., Fuhrer, O., Arteaga, A., Ban, N., Charpilloz, C., Di Girolamo, S., ... Wernli, H. (2020). Kilometer-scale climate models: Prospects and challenges. *Bulletin of the American Meteorological Society*, *101*(5), E567–E587. doi: 10.1175/BAMS-D-18-0167.1

Schmidt, G. A., Bader, D., Donner, L. J., Elsaesser, G. S., Golaz, J.-C., Hannay, C., ... Saha, S. (2017). Practice and philosophy of climate model tuning across six

US modeling centers. *Geoscientific Model Development*, *10*(9), 3207–3223. doi: 10.5194/gmd-10-3207-2017

Seneviratne, S. I., Corti, T., Davin, E. L., Hirschi, M., Jaeger, E. B., Lehner, I., ... Teuling, A. J. (2010). Investigating soil moisture–climate interactions in a changing climate: A review. *Earth-Science Reviews*, *99*(3-4), 125–161. doi: 10.1016/j.earscirev.2010.02.004

Shneerov, B. E., Meleshko, V. P., Matyugin, V. A., Sporyshev, P. V., Pavlova, T. V., Vavulin, S. V., ... Govorkova, V. A. (2001). Current State of the Main Geophysical Observatory Atmospheric General Circulation Model (MGO-2 version). In V. P. Meleshko & B. E. Shneerov (Eds.), *Proceedings of the voeikov main geophysical observatory* (Vol. 550, pp. 3–40). Saint Petersburg, Russia: Gidrometeoizdat. (In Russian. First canonical description of the MGO-2 (T42L14) spectral GCM, direct ancestor of the T42L25 configuration parallelized in this work)

Sundqvist, H., Berge, E., & Kristjánsson, J. E. (1989). Condensation and cloud parameterization studies with a mesoscale numerical weather prediction model. *Monthly Weather Review*, *117*(8), 1641–1657. doi: 10.1175/1520-0493(1989)117⟨1641:CACPSW⟩2.0.CO;2

Taylor, K. E. (2001). Summarizing multiple aspects of model performance in a single diagram. *Journal of Geophysical Research*, *106*(D7), 7183–7192. doi: 10.1029/2000JD900719

Tiedtke, M. (1989). A comprehensive mass flux scheme for cumulus parameterization in large-scale models. *Monthly Weather Review*, *117*(8), 1779–1800. doi: 10.1175/1520-0493(1989)117⟨1779:ACMFSF⟩2.0.CO;2

Tiedtke, M. (1993). Representation of clouds in large-scale models. *Monthly Weather Review*, *121*(11), 3040–3061. doi: 10.1175/1520-0493(1993)121⟨3040:ROCILS⟩2.0.CO;2

Trenberth, K. E. (1984). Some effects of finite sample size and persistence on meteorological statistics. Part I: Autocorrelations. *Monthly Weather Review*, *112*(12), 2359–2368. doi: 10.1175/1520-0493(1984)112⟨2359:SEOFSS⟩2.0.CO;2

Vokhmintsev, D. (2026a). *OpenMP parallelization of the MGO GCM with bitwise reproducibility: Thread-safe vertical exchange and deterministic spectral synthesis.* (Submitted to Journal of Parallel and Distributed Computing 2026-05-05;

preprint: `https://doi.org/10.2139/ssrn.6608580`; replication package: `https://doi.org/10.5281/zenodo.19653300`)

Vokhmintsev, D. (2026b). *Replication package for "Implicit-tuning Signal Quantified through a Tri-experiment Design in a Legacy Spectral GCM".* Zenodo. ([dataset]) doi: 10.5281/zenodo.20447240

Vokhmintsev, D. (2026c). *Replication package for "Quantifying the Memory Wall and Ensuring Reproducibility in a Legacy Spectral GCM".* Zenodo. ([dataset]) doi: 10.5281/zenodo.19653300

Voldoire, A., Saint-Martin, D., Sénési, S., Decharme, B., Alias, A., Chevallier, M., ... Waldman, R. (2019). Evaluation of CMIP6 DECK experiments with CNRM-CM6-1. *Journal of Advances in Modeling Earth Systems*, *11*(7), 2177–2213. doi: 10.1029/2019MS001683

Webb, M. J., Andrews, T., Bodas-Salcedo, A., Bony, S., Bretherton, C. S., Chadwick, R., ... Watanabe, M. (2017). The Cloud Feedback Model Intercomparison Project (CFMIP) contribution to CMIP6. *Geoscientific Model Development*, *10*(1), 359–384. doi: 10.5194/gmd-10-359-2017

Wilks, D. S. (2016). "the stippling shows statistically significant grid points": How research results are routinely overstated and overinterpreted, and what to do about it. *Bulletin of the American Meteorological Society*, *97*(12), 2263–2273. doi: 10.1175/BAMS-D-15-00267.1

Williamson, D. L. (2008). Convergence of aqua-planet simulations with increasing resolution in the Community Atmospheric Model, Version 3. *Tellus A: Dynamic Meteorology and Oceanography*, *60*(5), 848–862. doi: 10.1111/j.1600-0870.2008.00339.x

Young, A. H., Knapp, K. R., Inamdar, A., Hankins, W., & Rossow, W. B. (2018). The International Satellite Cloud Climatology Project H-Series climate data record product. *Earth System Science Data*, *10*(1), 583–593. doi: 10.5194/essd-10-583-2018

Zhang, G. J., & McFarlane, N. A. (1995). Sensitivity of climate simulations to the parameterization of cumulus convection in the Canadian Climate Centre general circulation model. *Atmosphere-Ocean*, *33*(3), 407–446. doi: 10.1080/07055900.1995.9649539

Zwiers, F. W., & von Storch, H. (1995). Taking serial correlation into account in tests

of the mean. *Journal of Climate*, *8*(2), 336–351. doi: 10.1175/1520-0442(1995)008⟨0336:TSCIAI⟩2.0.CO;2

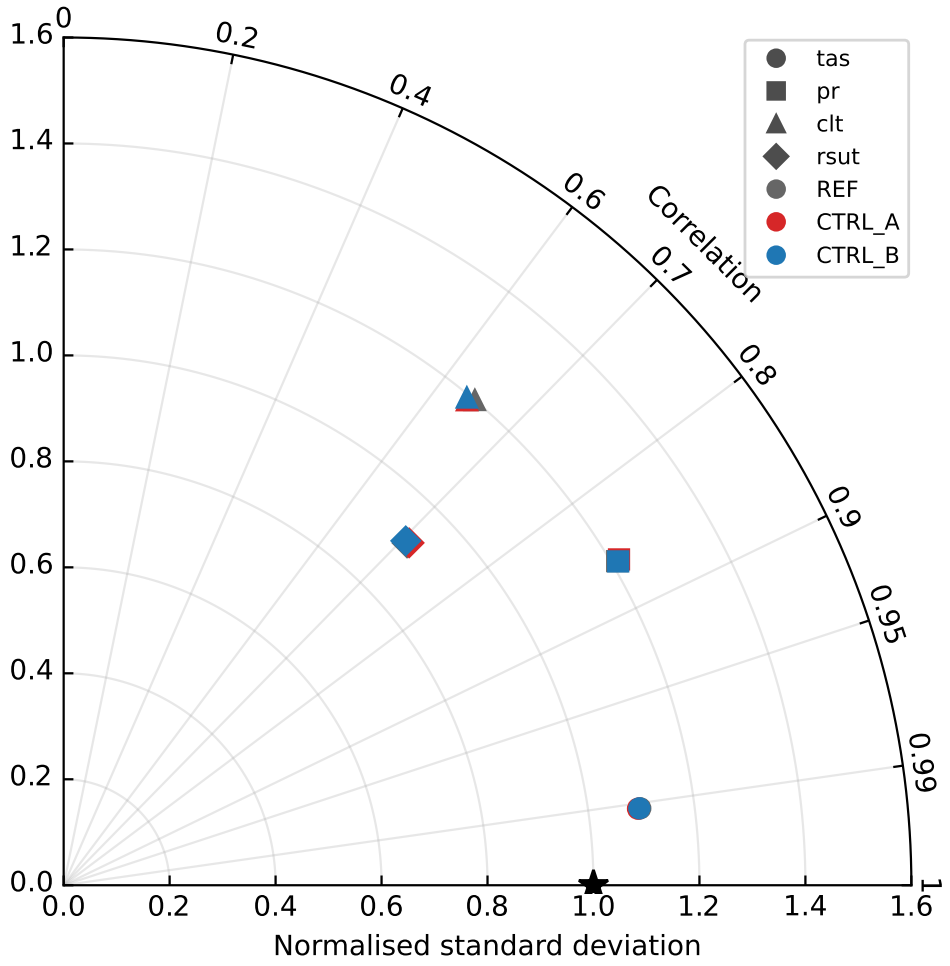

Figure 3. Taylor diagram of the annual-mean spatial fields against observations (`tas` vs ERA5, `pr` vs GPCP, `clt` vs ISCCP-H, `rsut` vs CERES EBAF) for REF, CTRL_A and CTRL_B. Radius is the normalised spatial standard deviation, azimuth the centred pattern correlation, and the star marks the observational reference. For every field the three configurations are nearly coincident, confirming that the implementation choice shifts amplitude and mean bias rather than spatial pattern.

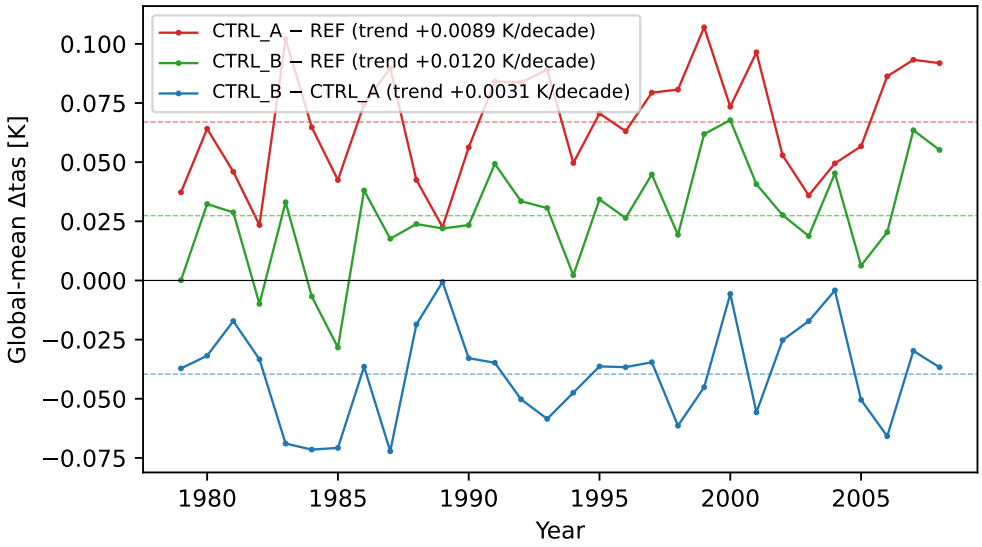

Figure 4. Ensemble-mean global-mean pairwise Δ`tas` per year (1979–2008) for the three contrasts; dashed lines mark the 30-year means and the legend reports the linear trend. The near-zero trends indicate that each contrast is stable across the integration rather than a transient equilibration artefact.

Supporting Information: Bitwise reproducibility theorem for the MGO atmospheric general circulation model

Dmitrii Vokhmintsev

June 13, 2026

This document accompanies the manuscript "Climate impact of eliminating spurious inter-latitude memory in the vertical exchange parameterization of the MGO atmospheric general circulation model (MGO-03 T42L25)" submitted to the *Journal of Advances in Modeling Earth Systems*. It contains the full statement and proof of the bitwise reproducibility theorem referenced in the main manuscript, together with supporting tables. Cross-references to numbered sections, tables, and figures refer to the main manuscript unless prefixed with "S".

Text S1: Pattern correlation of surface air temperature

Table S1 reports the cosine-of-latitude weighted spatial pattern correlation of simulated surface air temperature (`tas`) against ERA5, for the three configurations REF, CTRL_A and CTRL_B, at annual mean and for the four standard seasons, computed on the three-member initial-condition ensemble-mean climatology. The values support the statement in the Taylor-diagram discussion of the main manuscript that the configurations are essentially indistinguishable in angular position: the full range across all configurations and seasons is 0.9886 to 0.9921, and the maximum cross-configuration spread within any single period is 0.0001.

Table S1: Cosine-of-latitude weighted spatial pattern correlation of `tas` against ERA5 by configuration and period (three-member ensemble-mean climatology, 1979–2008).

Period	REF	CTRL_A	CTRL_B
Annual	0.9912	0.9912	0.9912
DJF	0.9921	0.9920	0.9921
MAM	0.9904	0.9905	0.9905
JJA	0.9886	0.9886	0.9886
SON	0.9897	0.9897	0.9896

Text S2: Inter-member consistency quantiles

Table S2 reports the area-weighted quantiles of the per-cell between-to-sampling variance ratio used in the inter-member consistency check of the main manuscript (Section 2.2), computed with the conservative effective-sample-size cap. The ratio is referred to a null distribution that is approximately $F(M-1, \sum_m (N_{\mathrm{eff},m}-1))$ with $M=3$ members, whose median is 0.70. The observed medians (0.57 and 0.67) and the full quantile spread lie at or below the null expectation, supporting the treatment of the three members as approximately independent replications.

Table S2: Area-weighted quantiles of the between-to-sampling variance ratio (capped N_{eff}) for the two leak-elimination contrasts, with the null-distribution median for reference.

Contrast	q_{10}	q_{25}	q_{50}	q_{75}	q_{90}	q_{95}	null median
CTRL_A−REF	0.084	0.231	0.567	1.206	2.069	2.790	0.70
CTRL_B−REF	0.093	0.272	0.668	1.359	2.308	3.095	0.70

0.1 Context and motivation

0.1.1 What the paper claims empirically

Section 4.1 of the companion paper introduces the per-J term-split reduction architecture (`COMSPE_PREJ_MOD`, `CVDDR_ACC_MOD`, `SPH_ACC_MOD`) and Section 4 introduces the `VE_JRESET` state-reset. Section 5 reports measured MD5 equalities of `tabm` across thread counts. The claim of strict IEEE-754 bitwise reproducibility across 1–16 threads is supported by three measured MD5 checksum tables:

- Zen 5: `84991763a21159cf30ccffad2e1287fb` for $N \in \{1, 2, 4, 8, 12, 16, 32\}$;
- Ivy Bridge-EP: `1322f6dad25e4011c2c4129881544c06` for $N \in \{1, \ldots, 24\}$.

0.1.2 What an attentive reviewer will ask

A natural reviewer objection is the following: an MD5 match on a one-month integration is evidence of determinism on that one-month window. Non-associativity of IEEE-754 addition implies that floating-point reorderings typically stay below machine epsilon per step but, in chaotic dynamical systems such as a general circulation model, may diverge to $O(1)$ after $\sim 10^2$–10^3 days. A one-month check is therefore insufficient to conclude that the implementation is *guaranteed* reproducible. Without a formal argument, the answer is "run longer and hope." With the theorem below, the answer is: bit-identity at step t is a deductive consequence of three implementation-level conditions, and extending the run length cannot produce divergence unless the implementation violates one of those conditions.

0.1.3 Related formal treatments

The question of bitwise reproducibility under parallel floating-point summation has a substantial literature. Compensated summation Kahan (1965) fixes a sequential order and is not directly applicable to the parallel case. He and Ding (2001) document floating-point divergence in parallel climate simulations empirically but do not prove conditions for bitwise identity. Demmel and Nguyen (2013) present reproducible summation algorithms via pre-rounding that guarantee order-independence; the present approach achieves order-independence by a different mechanism, fixing the reduction order rather than making the operator associative. Collange et al. (2015) introduce superaccumulators for multi-core reproducibility, and Iakymchuk et al. (2020) extend this to MPI+OpenMP solvers. The closest relative in spirit is the COSMO bit-reproducibility implementation by Schär et al. (2020), which limits compiler reorderings and parenthesises mathematical expressions in the source code so as to forbid the reassociation of summations and the creation of alternative execution strategies; the algorithmic foundation of reproducible reductions for general scientific applications is provided by Arteaga et al. (2014). The theorem below formalises the three conditions under which structural bit-reproducibility holds in our setting. A detailed comparison with algorithmic approaches (superaccumulators, pre-rounded reductions, canonical-order constructions) and a discussion of the diagnostic value of the structural approach are deferred to the companion methodological note in preparation.

0.2 Setting and notation

0.2.1 The model in abstract form

At time step t, the model state is a finite tuple of spectral coefficients

$$\mathbf{S}_t = \left(c_{\ell,m}^{(q)}(t)\right)_{\ell,m,q}, \tag{1}$$

where q indexes the five prognostic spectral fields (ζ, D, T, ℓ_z, ℓ_P): vorticity, divergence, temperature, the water-vapor field, and $\ell_P = \ln p_s$ (the logarithmic surface pressure); see Sect. 3.2 of the companion paper for the model-specific scaling of the water-vapor variable. Here $\ell = 0, \ldots, M$ is the total wavenumber, $|m| \le \ell$ is the zonal wavenumber, and $M = 42$ is the triangular truncation. Each coefficient is a finite-length IEEE-754 double-precision value (`REAL*8`).

0.2.2 The per-time-step update

One time step of the model factors as

$$\mathbf{S}_{t+1} \;=\; \mathcal{F}(\mathbf{S}_t) \;=\; \mathcal{L}(\mathbf{S}_t) \;+\; \sum_{J=1}^{J_M} \mathbf{\Delta}^{(J)}(\mathbf{S}_t), \tag{2}$$

where:

- $\mathcal{L}(\mathbf{S}_t)$ is the *linear* spectral-space update (horizontal diffusion, pressure gradient, Coriolis force, semi-implicit gravity-wave term). It does not depend on J; by construction it is a deterministic IEEE-754 function of $\mathbf{S}_t$.
- $\mathbf{\Delta}^{(J)}(\mathbf{S}_t)$ is the *grid-space* tendency contribution from latitude J. It collects the outputs of physical parameterizations (radiation, convection, vertical exchange, turbulence) projected back to spectral space via FFT plus Legendre transform and summed into the global coefficient array.
- $J_M = 32$ for T42 (half the Gaussian grid, exploiting equatorial symmetry).

The summation $\sum_{J=1}^{J_M}$ in Eq. (2) is the *spectral synthesis reduction* of Sect. 4.1. Its evaluation order is the subject of the theorem.

0.2.3 The parallel execution model

For thread count $N \in \{1, 2, \ldots, J_M\}$, the J_M iterations are partitioned across N OpenMP threads. Let $\mathcal{P}_N(J) \in \{0, \ldots, N-1\}$ denote the thread that evaluates latitude J under an OpenMP `static` schedule. Thread affinity to physical cores is fixed (`OMP_PROC_BIND=close`, `OMP_PLACES=cores`), but the exact binding is not part of the theorem.

0.2.4 IEEE-754 determinism (assumption A0)

We assume throughout that the compiled binary executes under a fixed IEEE-754 rounding mode (round-to-nearest-even) and that no reordering transformation is applied by the hardware or the compiler beyond what is compatible with the IEEE-754 semantics of the source text. Concretely:

- The theorem applies to the CTRL_A and CTRL_B configurations, which are compiled with `-O2 -march=native`; REF is excluded from the theorem's scope because it violates condition (C2) through the inter-latitude state leakage documented in Section 2.2 of the main text. Under `-O2 -march=native`, FMA is allowed: FMA contracts $a \cdot b + c$ into a single rounding (distinct from separate `mul`+`add`), but this contraction is deterministic: the same source expression compiles to the same FMA on every run.

- Hardware non-associativity (e.g. reorder buffers) does not change the functional output of an individual instruction.

- External sources of non-determinism are eliminated by design: no random number generation is used by the model initialization in the reproducibility runs, all input files (SST/SIC, aerosol forcing) are byte-identical across runs, and clocks/timers are read only in non-reducing contexts (e.g. diagnostic prints that do not feed back into $\mathbf{S}$).

Under (A0), the output of each arithmetic primitive (addition, multiplication, FMA, division, square root) is a deterministic function of its operands. This is the bedrock of everything that follows: once we fix *which* operands enter each primitive, *in what order*, the bitstream of results is fully determined.

0.3 The three structural conditions

0.3.1 (C1) Ordered per-J reduction

The spectral synthesis reduction is evaluated as a fixed sequential sum

$$c_{\ell,m} \leftarrow c_{\ell,m}^{\mathrm{LIN}} \oplus \Delta c_{\ell,m}^{(1)} \oplus \Delta c_{\ell,m}^{(2)} \oplus \cdots \oplus \Delta c_{\ell,m}^{(J_M)}, \tag{3}$$

where $\oplus$ is IEEE-754 addition with left-to-right associativity $((a \oplus b) \oplus c) \oplus d$, and the *summation is performed in a single thread* (the OpenMP master, inside the `!$OMP MASTER` region of `sph_cm-19_r2.F`) *after* all threads have completed their per-latitude work and deposited their $\Delta c_{\ell,m}^{(J)}$ into disjoint slots of per-J buffer arrays. This condition is independent of N: the reduction loop reads slots $J = 1, 2, \ldots, J_M$ sequentially, always in that order.

Code implementing (C1):

- `comspe_prej_mod.f90` – subroutine `COMSPE_PREJ_REDUCE` (serial ordered sum of five spectral fields over J);

- `cvddr_acc_mod.f90` – subroutine `CVDDR_ACC_FINALIZE` (serial ordered sum of vertical-diffusion diagnostics);

- `sph_acc_mod.f90` – subroutine `SPH_ACC_FINALIZE` (serial ordered sum of `AIN_MOD` scalar diagnostics together with seven `REAL*4` arrays).

0.3.2 (C2) State isolation (VE_JRESET)

For every J-iteration, all `THREADPRIVATE` working arrays of every subroutine called inside the J-loop are reset to a deterministic initial state before the J-th evaluation. The initial state is either zero (for accumulators) or a designated neutral value (e.g. BETA = 1, FVT = 1 in the vertical-exchange kernel; see the `VE_JRESET` entry in the project journal).

Code implementing (C2):

- `ve_r2.F` – `VE_JRESET`: explicit zeroing of the 25 `MEMORIZED` arrays (`ZHR12`, `DZR12`, `ALR9`, `ALR12`, `FUNCM`, `FUNCH`, `TKEK`, `RKZ`, `ALFTKE`, `BETTKE`, `AKM12`, `AKH12`, etc.) at the top of every `VE` entry;

- `comspe_prej_mod.f90` – subroutine `COMSPE_PREJ_INIT` called before `!$OMP PARALLEL DO` each time step;

- `cvddr_acc_mod.f90` – subroutine `CVDDR_ACC_INIT` called before `!$OMP PARALLEL DO`;

- `sph_acc_mod.f90` – subroutine `SPH_ACC_INIT` called before `!$OMP PARALLEL DO`.

0.3.3 (C3) Disjoint writes

Within a single J-iteration, the set of memory addresses written by thread $\mathcal{P}_N(J)$ is disjoint from the set of memory addresses written by any other thread $\mathcal{P}_N(J')$ with $J' \neq J$. In particular:

- per-J buffer arrays (`COMSPE_PREJ_MOD::YLPC_J(:,J)`, `CVDDR_ACC_MOD::GRM2_J(J)`, `SPH_ACC_MOD::EK_J(J)`, etc.) are indexed by the latitude J of the writing thread; no other thread writes to the same J-slice;
- `THREADPRIVATE` arrays are, by definition, distinct memory per thread;
- shared read-only data (grid constants, input boundary conditions) is not written.

Code implementing (C3):

- `!$OMP PARALLEL DO SCHEDULE(STATIC) DEFAULT(NONE)` in `sph_cm-19_r2.F` line 549, with explicit `SHARED/PRIVATE/FIRSTPRIVATE/THREADPRIVATE` classification of every variable in scope ($\sim$60 classified names; see `sph_cm-19_r2.F` lines 458–507);
- the `DEFAULT(NONE)` clause guarantees at compile time that no variable is accidentally shared; the explicit classification makes the write-disjoint property a structural property of the code rather than an accident of optimization.

0.4 Theorem statement

0.4.1 Single-step version

Theorem 1 (Single-step bitwise reproducibility)**.** *Let $\mathbf{S}_t$ be the state at time step t. Under assumption* (A0) *of IEEE-754 determinism and conditions* (C1)*,* (C2)*, and* (C3)*, the state at time step $t+1$ computed by the parallelized binary is bit-identical for every thread count $N \in \{1, 2, \ldots, J_M\}$ on the same hardware-compiler configuration:*

$$\forall\, N, N' \in \{1, \ldots, J_M\} : \quad \mathbf{S}_{t+1}^{(N)} \;=\; \mathbf{S}_{t+1}^{(N')}. \tag{4}$$

0.4.2 Inductive version

Theorem 2 (Multi-step bitwise reproducibility)**.** *Under the same assumptions, if $\mathbf{S}_0^{(N)} = \mathbf{S}_0^{(N')}$ (identical initialization, typically from the same restart file), then*

$$\forall\, t \geq 0,\ \forall\, N, N' \in \{1, \ldots, J_M\} : \quad \mathbf{S}_t^{(N)} \;=\; \mathbf{S}_t^{(N')}. \tag{5}$$

Consequently, every diagnostic output file derived from $\mathbf{S}_t$ by a deterministic post-processing map (e.g. `tabm`, `tabv`, `tabcltm`, the `lst` logs) is byte-identical across thread counts.

0.4.3 Scope of "the same hardware-compiler configuration"

Theorems 1 and 2 assume that the executable binary, its libgomp/libm implementations, the CPU microarchitecture, and the memory subsystem produce the same IEEE-754 output for each arithmetic primitive. They do *not* claim bit-identity across different binaries (e.g. Zen 5 with `-march=znver5` vs. Ivy Bridge-EP with `-march=ivybridge`), because the compilers generate different instruction sequences (FMA on Zen 5, separate `mul`+`add` on Ivy Bridge). Within a single binary executed on the target hardware, however, Theorems 1 and 2 hold for every N. The measured cross-platform MD5s (`84991763...` on Zen 5 and `1322f6da...` on Ivy Bridge-EP) are therefore an *expected* consequence, not a violation, of Theorem 2.

0.5 Sketch of proof

The argument is given here in outline; the full proof, together with a detailed discussion of the diagnostic value of (C1)–(C3) and the scope of validity of the theorem, is presented in the companion methodological note in preparation.

For Theorem 1, fix a thread count N and state $\mathbf{S}_t$. The linear update $\mathcal{L}(\mathbf{S}_t)$ is evaluated outside the J-loop and is deterministic by (A0). For each latitude J, the tendency $\mathbf{\Delta}^{(J)}(\mathbf{S}_t)$ is a function only of J and $\mathbf{S}_t$: condition (C2) eliminates hidden dependency on the history of previous J-iterations, and condition (C3) eliminates dependency on concurrent activity of other threads. The reduction $c_{\ell,m}^{\mathrm{LIN}} \oplus \Delta c_{\ell,m}^{(1)} \oplus \cdots \oplus \Delta c_{\ell,m}^{(J_M)}$ is then evaluated by (C1) in a fixed left-to-right order in a single thread, and is therefore byte-identical for every N.

Theorem 2 follows by induction on t: the base case $t = 0$ is identical initial conditions by assumption, and the inductive step is Theorem 1 applied to a state already byte-identical across thread counts by the inductive hypothesis. Chaotic divergence cannot enter because there is no perturbation to amplify; the iteration starts each step from the same state, not from an ϵ-perturbed one.

0.6 Empirical validation and residual evidence

The theorem makes a specific prediction: bit-identity at *every* time step for *every* thread count. The companion paper validates this prediction on two different scales:

- *Time-step level.* Section 5 of the companion paper reports MD5 equality of `tabm` at the end of a one-month integration ($\sim$2 000 time steps of 22.5 min each). Independent testing in the engineering log has extended this check to twelve-month runs at 1T and 6T with identical MD5.
- *Thread-count level.* MD5 identity across $N \in \{1, 2, 4, 8, 12, 16, 32\}$ on Zen 5 and $N \in \{1, 2, 4, 8, 12, 16, 24\}$ on Ivy Bridge-EP. The two platforms produce distinct MD5s (different `-march` binaries), but each is internally bit-stable across all N, which is the theorem's claim.

The empirical agreement is not evidence *for* the theorem (the theorem is deductively true given its premises); it is evidence that the implementation *satisfies* the premises. The engineering work is in checking (C1)–(C3), not in rederiving Theorem 1.

0.7 Companion standalone note

The present Supporting Information provides the theorem statements, a sketch of proof, and the MGO empirical verification needed to support the climate-impact analysis of the main manuscript. A companion methodological note is in preparation for separate submission to the numerical-software literature (ACM Transactions on Mathematical Software). That note presents the full formal proof, a detailed comparison with algorithmic approaches to bit-reproducibility (superaccumulators, pre-rounded reductions, canonical-order constructions), a discussion of the diagnostic value of the three conditions for catching inter-iteration state-leakage bugs, and a theoretical-applicability discussion for other spectral atmospheric general circulation models. The companion note targets the numerical-software community; the present Supporting Information is integral to the climate-impact analysis of this manuscript.

Text S3: Mapping of theorem conditions to replication-package source

The bitwise-reproducibility theorem rests on three structural conditions (C1)–(C3). Table S3 maps each condition to the specific source files and routines that implement it. All listed files

are contained in the openly archived diff/patch package (paths relative to `src_mgo/atm-77_r2/`); they are self-contained with respect to the conditions and allow a reviewer to verify (C1)–(C3) without access to the proprietary base model. Line numbers refer to the archived package version.

Table S3: Source-level provenance of the three reproducibility conditions. Routines reside in the deterministic-reduction modules and the vertical-exchange kernel; all are part of the public diff/patch package.

Condition	File	Routine (line)	Role
(C1) Ordered per-J reduction	`gcm/comspe_prej_mod.f90`	`COMSPE_PREJ_REDUCE` (L107)	Ordered sum of five spectral fields over J
	`gcm/cvddr_acc_mod.f90`	`CVDDR_ACC_FINALIZE` (L201)	Ordered sum of diffusion diagnostics
	`gcm/sph_acc_mod.f90`	`SPH_ACC_FINALIZE` (L149)	Ordered sum of `AIN_MOD` scalars and seven `REAL*4` arrays
(C2) State isolation	`gcm/ve_r2.F`	`VE_JRESET` (L634–907)	Per-J zeroing of 25 `MEMORIZED` arrays
	`gcm/comspe_prej_mod.f90`	`COMSPE_PREJ_INIT` (L85)	Reset before `!$OMP PARALLEL DO`
	`gcm/cvddr_acc_mod.f90`	`CVDDR_ACC_INIT` (L155)	Reset before `!$OMP PARALLEL DO`
	`gcm/sph_acc_mod.f90`	`SPH_ACC_INIT` (L111)	Reset before `!$OMP PARALLEL DO`
(C3) Disjoint writes	`gcm/comspe_prej_mod.f90`	`YLPC_J(:,J)`	Per-J buffer slice indexed by the writing thread's J
	`gcm/cvddr_acc_mod.f90`	`GRM2_J(J)`	Per-J buffer slice
	`gcm/sph_acc_mod.f90`	`EK_J(J)`	Per-J buffer slice; other work arrays `THREADPRIVATE`

References

Andrea Arteaga, Oliver Fuhrer, and Torsten Hoefler. Designing bit-reproducible portable high-performance applications. In *Proceedings of the 28th IEEE International Parallel and Distributed Processing Symposium (IPDPS)*, pages 1235–1244, Phoenix, AZ, USA, 2014. IEEE. doi: 10.1109/IPDPS.2014.127.

Sylvain Collange, David Defour, Stef Graillat, and Roman Iakymchuk. Numerical reproducibility for the parallel reduction on multi- and many-core architectures. *Parallel Computing*, 49:83–97, 2015. doi: 10.1016/j.parco.2015.09.001.

James Demmel and Hong Diep Nguyen. Fast reproducible floating-point summation. In *Proceedings of the 21st IEEE Symposium on Computer Arithmetic (ARITH)*, pages 163–172, Austin, TX, USA, 2013. IEEE. doi: 10.1109/ARITH.2013.9.

Y He and C Ding. Using accurate arithmetics to improve numerical reproducibility and stability in parallel applications. *The Journal of Supercomputing*, 18(3):259–277, 2001. doi: 10.1023/A:1008153532043.

Roman Iakymchuk, Maria Barreda Vayá, Stef Graillat, José I Aliaga, and Enrique S Quintana-Ortí. Reproducibility of parallel preconditioned conjugate gradient in hybrid programming environments. *The International Journal of High Performance Computing Applications*, 34(5):502–518, 2020. doi: 10.1177/1094342020932650.

William Kahan. Further remarks on reducing truncation errors. *Communications of the ACM*, 8 (1):40, 1965. doi: 10.1145/363707.363723.

Christoph Schär, Oliver Fuhrer, Andrea Arteaga, Nikolina Ban, Christophe Charpilloz, Salvatore Di Girolamo, Laureline Hentgen, Torsten Hoefler, Xavier Lapillonne, David Leutwyler, Katherine Osterried, Davide Panosetti, Stefan Rüdisuhli, Linda Schlemmer, Thomas C. Schulthess, Michael Sprenger, Stefano Ubbiali, and Heini Wernli. Kilometer-scale climate models: Prospects and challenges. *Bulletin of the American Meteorological Society*, 101(5):E567–E587, 2020. doi: 10.1175/BAMS-D-18-0167.1.